A frustrated [Mn_{18}] wheel-of-wheels

Marco Coletta,[a] Thomais G. Tziotzi,[b] Mark Gray,[a] Gary S. Nichol,[a] Mukesh K. Singh,*[a] Constantinos J. Milios*[b] and Euan K. Brechin*[a]

[a]EaStCHEM School of Chemistry, The University of Edinburgh, David Brewster Road, Edinburgh, EH9 3FJ, UK. Email: E.Brechin@ed.ac.uk; mklsingh36@gmail.com

[b]Department of Chemistry, The University of Crete, Voutes, 71003, Herakleion, Greece. Email: komil@uoc.gr

Abstract

A [Mn_{18}] wheel of wheels is obtained from the reaction of $MnBr_2$ and LH_3 in MeOH. The metallic skeleton reveals two asymmetric [$Mn^{III}_6Mn^{II}_2$] squares connected into a wheel via two apical Mn^{II} ions. Magnetic susceptibility and magnetisation data reveal competing exchange interactions, supported by computational studies revealing spin frustration.

Introduction

Beyond beautiful structural aesthetics, wheels of paramagnetic metal ions have proven to be vital for revealing quantum effects,[1] constructing very high spin molecules,[2] engineering toroidal magnetic moments,[3] developing magnetic Möbius strips,[4] understanding frustration effects,[5] probing slow magnetisation relaxation,6 investigating quantum information processing,[7] and developing magneto-structural correlations.[8] In Mn coordination chemistry wheels have presented nuclearities as large as eighty-four,[9] displaying a variety of topologies constructed from chains of single metal ions and polymetallic building blocks.[10-13] Amongst ligand types, those containing one or more ethanolamine (eaH) moieties (Figure 1) have proven enormously successful in building a breadth of structurally and magnetically fascinating species.[14] Herein we extend this body of work to include the ligand 1,3,5-tri(2-hydroxyethyl)-1,3,5-triazacyclohexane (LH_3), which contains three linked eaH units. A search of the Cambridge Structural Database (CSD) reveals just four hits in 3d transition metal chemistry. The first was the monomer [$Cr(CO)_3(LH_3)$],[15] the second an aesthetically pleasing [Mn_{16}] complex in which the ligand was generated serendipitously in-situ,[16] and the third and fourth structurally related [Mn_{16}] and [Mn_{10}] square wheels.[17]

Results and Discussion

Reaction of $MnBr_2{\cdot}4H_2O$ with LH_3 in MeOH affords black crystals of [$Mn^{III}_{12}Mn^{II}_6(O)_6(OH)_2(OMe)_6(L)_4(LH)_2Br_{12}$] (**1**, Figure 2, S1-4) after 2 days (see SI for full experimental details). Compound **1** crystallises in the monoclinic space group *I*2/*a*, with half the complex in the asymmetric unit (ASU). The metallic skeleton of **1** describes two puckered, square [$Mn^{III}_6Mn^{II}_2$] wheels (Mn1-7) linked via two apical Mn^{II} ions (Mn8). The [$Mn^{III}_6Mn^{II}_2(\mu_3\text{-}O)_6(\mu\text{-}OH)_2(OMe)_6$] core of the squares is asymmetric (Figure 2). Three of the four corners (Mn1-3, Mn3-5, Mn5-7) are bridged 'internally' via a 'T-shaped' $\mu_3\text{-}O^{2-}$ ion (O11-O13) and two externally via a $\mu\text{-}OMe^-$ ion (Mn1-O15-Mn2, Mn6-O16-Mn7). The fourth corner (Mn1, Mn7, Mn9) is connected only 'internally' via one $\mu_3\text{-}OMe^-$ ion (O14) and one μ–OH^- ion (O10). The Mn^{II} ions (Mn4, Mn9) occupy opposite vertices in the square, sandwiched between the two [$Mn^{III}3$] triangles (Mn1-3, Mn5-7). There are two μ_6-L and one μ_5-LH ligands in the ASU. The former sit above a [Mn^{III}_3] triangle which acts as the corner of the square, each atom coordinated to a different Mn^{III} ion.

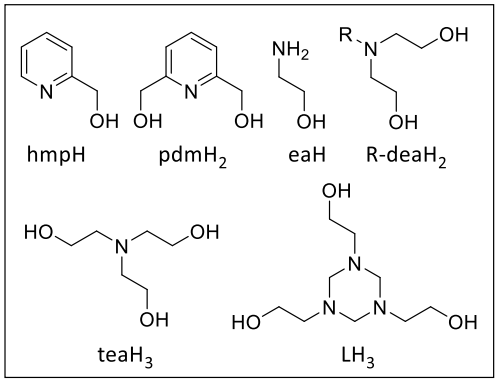

Figure 1. The N,O-chelates 2-(hydroxymethyl)pyridine (hmpH), 2,6-pyridinedimethanol ($pdmH_2$), di- (R-$deaH_2$) and triethanolamine ($teaH_3$), and 1,3,5-tri(2-hydroxyethyl)-1,3,5-triazacyclohexane (LH_3), all of which contain one or more linked ethanolamine (eaH) moieties.

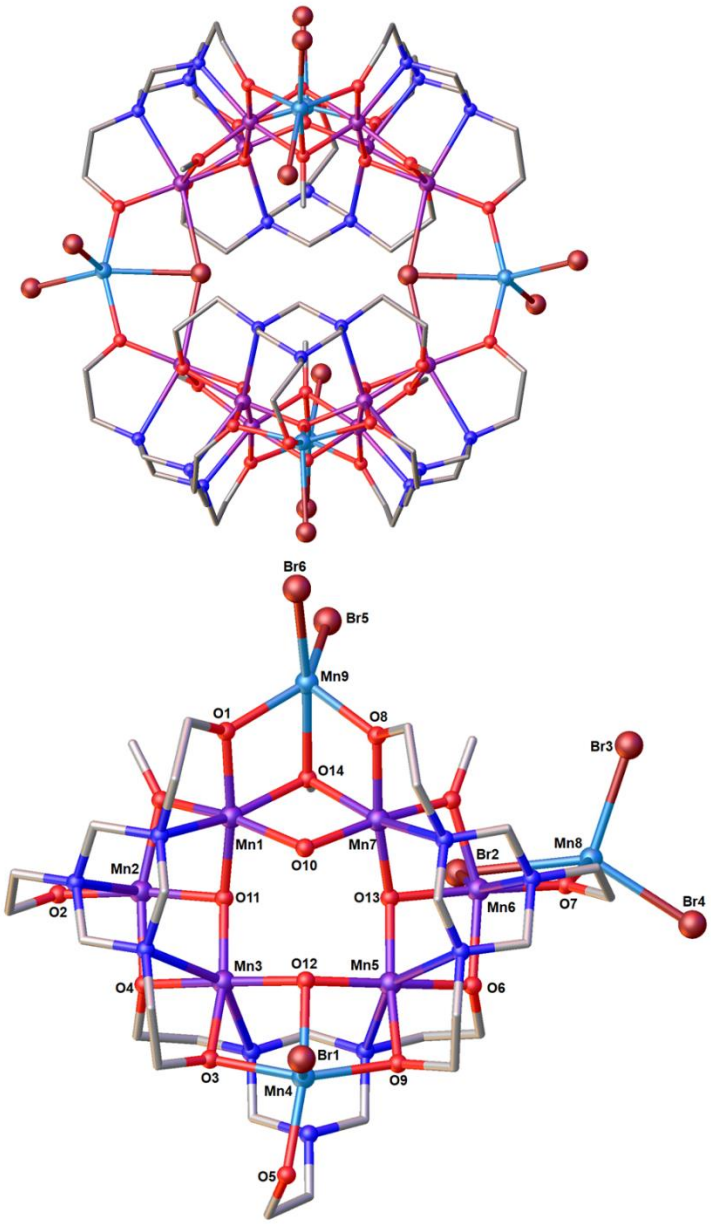

Figure 2. The molecular structure of **1** (top) and the labelled ASU (bottom). Colour code: Mn^{III} = purple, Mn^{II} = light blue, O = red, N = dark blue, C = grey, Br = brown.

The O-atoms also bond to the same metal ion but further μ–bridge to a neighbouring Mn^{II} ion in the square (Figure S2). The LH ligands sit above the [$Mn^{III}2Mn^{II}$] square corner with each N-atom coordinated to a different Mn ion. Two of the three O-arms μ–bridge to a neighbouring Mn^{III} ion in the square, with the third O-arm (O5) terminally bonded to a Mn^{II} ion (Figure S3). The two μ_3-Br^- ions (Br2 and symmetry equivalent, s.e.) are bonded to the apical Mn^{II} ions (Mn8) and link the two halves of the cluster together bridging between Mn2 and Mn6 (and s.e.). Mn8 is 5-coordinate and in pentagonal bipyramidal geometry, it's $\{MnO_2Br_5\}$ coordination sphere being completed with two monodentate Br ions. Mn9 is coordinated in a similar fashion, but Mn4 is square pyramidal and bonded to just one Br ion and possesses a $\{MnO_4Br\}$ coordination sphere. Thus, the Mn^{II} sites are easily distinguished by being bonded to Br ions. The six Mn^{III} ions in the ASU (Mn1-3, Mn5-7) are all in Jahn-Teller (JT) distorted octahedral geometries (Figure S4), which are also easily distinguished since they all involve the triazacyclohexane ring N-atoms. The closest inter-molecular interactions occur between the terminally bonded Br ions and the C-atoms of the triazacyclohexane ring (C···N ≥ 3.85 Å) directing the formation of columns of **1** in the extended structure along the a-axis of the cell (Figure S5). A search of the Cambridge Structural Database reveals that seventeen [Mn_{18}] clusters have been reported previously, but none have the topology seen in **1**. We note that there are some structural similarities to the [Mn_{16}] and [Mn_{10}] clusters we previously reported with this ligand, both of which describe wheel-like structures built from [Mn_3] triangular building blocks as directed by the coordination of the triazatriol ligand.[17]

The magnetic properties of a freshly prepared polycrystalline sample of **1** were measured in an applied field, B = 0.5 T, over the T = 2-300 K temperature range. The experimental results are showed in Figure 3, in the form of the $\chi_M T$ product, where $\chi_M = M/B$, and M is the magnetisation of the sample. At room temperature the $\chi_M T$ product of 1 (50.43 cm^3 K mol^{-1}) is lower than the sum of the Curie constants expected for a [$Mn^{III}_{12}Mn^{II}_6$] (62.25 cm^3 K mol^{-1}) unit. As temperature decreases, the $\chi_M T$ first decreases a value of 41.20 cm3 K mol-1 at T = 60 K, before increasing to a maximum of 44.70 cm^3 K mol^{-1} at 11 K, and then falls to a value of 26.00 cm^3 K mol^{-1} at T = 2 K. This behaviour is clearly indicative of competing exchange interactions, with the increase between 60-11 K perhaps suggestive of ferromagnetic exchange between the two square [$Mn^{III}_6Mn^{II}_2$] wheels. The decrease in $\chi_M T$ at the lowest temperatures is attributed to a combination of intra- and intermolecular antiferromagnetic exchange and zero field splitting (*zfs*) effects. Low temperature variable-temperature-and-variable-field (VTVB) magnetisation data were measured in the temperature range 2–7 K, in magnetic fields up to 7.0 T (Figure 3, inset; Figure S6). At the lowest temperature and highest field measured, M reaches a value of ~37 μ_B but does not saturate. There are no out-of-phase signals in ac susceptibility measurements in zero dc field.

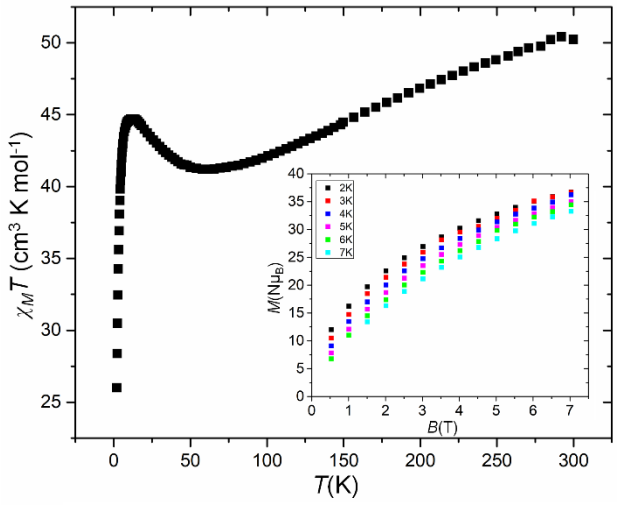

Figure 3. Temperature dependence of the $\chi_M T$ product for **1** collected in an applied magnetic field of B = 0.5 T. The inset shows the VTVB magnetisation data in the temperature/field ranges 2–7 K / 0.5 – 7 T.

Since the nuclearity of **1** precludes a fit of the experimental data via standard techniques, we have calculated the magnetic exchange interactions using computational tools known to accurately reproduce experimental *J* values (see the computational details section in the ESI for more details).[18] We have performed calculations on a model complex, **1a**, which is simply the ASU, *i.e.* one [$Mn^{III}_6Mn^{II}_2$] wheel plus one linking Mn^{II} ion (Figure S7). Based on symmetry and the different bridging groups/angles present, the number of unique magnetic exchange interactions can be reduced to six (Table S1, Figure S8). These are: (J_1) Mn^{III}-Mn^{III} mediated through μ_3-O^{2-} and μ-OR; (J_2) Mn^{III}-Mn^{III} mediated through μ_3-O^{2-}; (J_3) Mn^{III}-Mn^{III} mediated through μ-OH and μ_3-OR; (J_4) Mn^{II}-Mn^{III} mediated through μ_3-O^{2-} and μ-OR; (J_5) Mn^{II}-Mn^{III} mediated through μ-OR and μ_3-OR, and (J_6) Mn^{II}-Mn^{III} mediated through μ-Br and μ-OR (Figure 4, Figure S8).

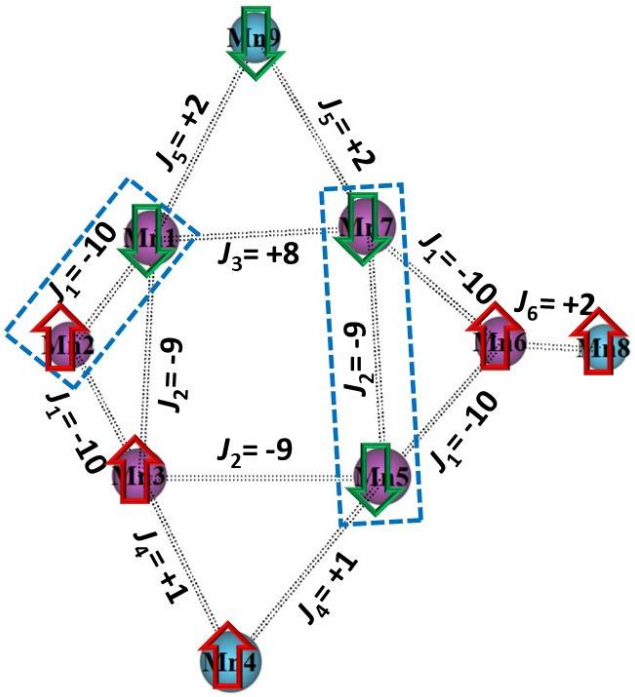

Figure 4. DFT calculated magnetic exchange interactions (J_1-J_6 / cm^{-1}) for **1** together the ground state spin orientation for model **1a**. The red and green arrows represent spin-up and spin-down, respectively. The blue dotted squares show the magnetic centres exhibiting spin frustration.

The first two interactions (J_1 and J_2) are found to be anti-ferromagnetic, whereas the remaining four interactions, (J_3-J_6) are estimated to be ferromagnetic (Figure 4, Figures S8-9, Table S1). For the J_1 interaction, the JT axis of both Mn^{III} ions are found to be collinear and perpendicular to the bridging plane of the dimer (Figure 5, Figure S10a). According to the magnetostructural correlation for [Mn^{III}_2] dimers discussed in reference 19 this describes a Type I geometry that should lead to antiferromagnetic exchange.[19] Overlap integral (|Sab|) calculations are in agreement, with two strong and four intermediate interactions detected, leading to a relatively strong antiferromagnetic interaction, J_1 = - 10 cm-1 (Table S2, Figure S11a-f). For the J_2 interaction, the Mn^{III} ions are bridged via μ_3-O^{2-} ions with Mn-μ_3O-Mn angles between 132-136°. Overlap calculations suggests one strong and four intermediate interactions (Table S1, Figure S11g-k), leading to a relatively strong antiferromagnetic interaction, J_2 = -9 cm^{-1}. For the J_3-J_6 interactions, overlap integral calculations reveal that only intermediate interactions are observed, resulting in ferromagnetic exchange coupling with J_3 = +8 cm^{-1}, J_4 = +1 cm^{-1}, J_5 = +2 cm^{-1} and J_6 = +2 cm^{-1} (Table S1, Figure S11l-w). These values are in-line with those previously reported for similar bridging moieties, and consistent with published magneto-structural studies.[20] The magnitude and sign of the magnetic exchange interactions can also be related to the calculated average total overlap integral (∑|Sa(3d)b(3d)|/n, Figure S12).[21] The smaller the average total overlap integral, the larger the ferromagnetic interaction (or the smaller the antiferromagnetic interaction) and vice versa. Note that for the J_3 interaction, the JT axes of the Mn^{III} ions lie perpendicular to each other, with one lying parallel to the bridging plane and the other perpendicular to the bridging plane. This is a Type

III geometry (Figure 5, Figure S10b), and would be expected to promote ferromagnetic exchange.[19] The J_1-J_4 interactions between $Mn^{III/II}$-Mn^{III} centres are also mediated via the $(R_2)N\text{-}CH_2\text{-}N(R_2)$ group of the triazatriol ligand (Table S1). However, the expected contribution to the total magnetic exchange through this long bridging group would be expected to be minimal, and indeed the calculated spin density on the connecting -CH_2- group is close to zero (≤ 0.003, Figure S13) breaking any spin delocalisation/polarisation pathway. A summary of these results is shown in Figure 4 alongside a cartoon of the "spin-up" / "spin-down" orientations of the individual Mn ions in **1a**. In an isotropic model this would lead to a frustrated spin ground state of S = 5.

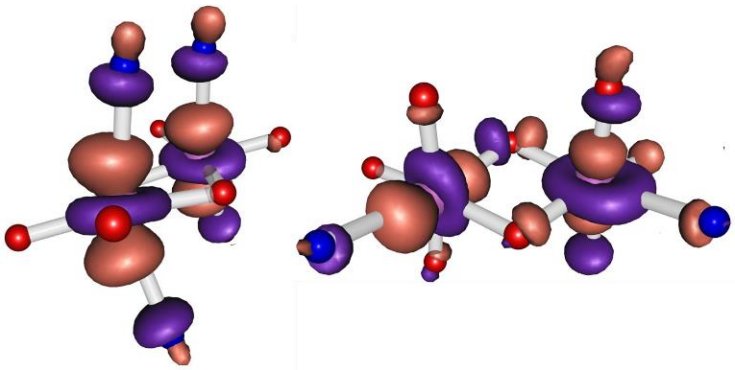

Figure 5. Schematic presentation of Jahn-Teller axis for (left) {Mn5-Mn6, J_1} and (right) {Mn1-Mn7, J_3}. For J_1 the Jahn-Teller axes of the Mn^{III} ions are found to be collinear and perpendicular to the bridging plane of the dimer (Type I). For J_3 the Jahn-Teller axes of the Mn^{III} ions are perpendicular to each other with one lying parallel to the bridging plane and the other perpendicular to the bridging plane (Type III).

In summary, the simple reaction between $MnBr_2{\cdot}4H_2O$ with LH_3 in MeOH affords the species $[Mn^{III}{}_{12}Mn^{II}{}_6(O)_6(OH)_2(OMe)_6(L)_4(LH)_2Br_{12}]$, **1**. The metal core of **1** consists of two square $[Mn^{III}{}_6Mn^{II}{}_2]$ wheels linked via two Mn^{II} ions. The wheels incorporate four vertex sharing triangles, which leads to spin frustration, while the link between wheels is ferromagnetic leading to a non-zero spin ground state. Given the lack of base in the reaction, the full deprotonation of four out of six ligands, and the double deprotonation of the remaining two, is intriguing. We speculate that full deprotonation and the conversion of the hydroxides to oxides may lead to a more symmetric wheel, or wheel of wheels, while oxidation of the Mn^{II} ions should also result in significant structural rearrangement. It is also interesting to note that in all the Mn complexes we have isolated with LH_3 thus far[17] – $[Mn_{10}]$, $[Mn_{16}]$ and $[Mn_{18}]$ – the direction of the JT axes of the Mn^{III} ions is dictated by the triaza N-atoms (*i.e.* perpendicular to the triaza macrocycle). This has important consequences for controlling nearest neighbour magnetic exchange interactions and thus needs to be carefully considered in future design.

Acknowledgements

We thank the EPSRC for financial support under grant reference numbers EP/N01331X/1, and the Marie Skłodowska-Curie actions (MSCA) for grant MMQIP 832488 (to MKS). Crystallographic data for 1 were measured remotely at beam line I-19 of Diamond Light Source (award CY22240).

Conflicts of interest

There are no conflicts to declare.

Notes and references

1 K. L. Taft, C. D. Delfs, G. C. Papaefthymiou, S. Foner, D. Gatteschi and S. J. Lippard, *J. Am. Chem. Soc*., 1994, **116**, 823– 832.

2 A. Baniodeh, N. Magnani, Y. Lan, G. Buth, C. E. Anson, J. Richter, M. Affronte, J. Schnack and A. K. Powell, *npj Quant. Mater*., 2018, **3**, 10.

3 L. Ungur, S. K. Langley, T. N. Hooper, B. Moubaraki, E. K. Brechin, K. S. Murray and L. F. Chibotaru, *J. Am. Chem. Soc*., 2012, **134**, 18554–18557.

4 O. Cador, D. Gatteschi, R. Sessoli, F. K. Larsen, J. Overgaard, A.-L. Barra, S. J. Teat, G. A. Timco and R. E. P. Winpenny, *Angew. Chem. Int. Ed*., 2004, **43**, 5196-5200.

5 M. L. Baker, G. A. Timco, S. Piligkos, J. S. Mathiesone, H. Mutka, F. Tuna, P. Kozłowskif, M. Antkowiakf, T. Guidi, T. Gupta, H. Rath, R. J. Woolfson, G. Kamieniarz, R. G. Pritchard, H. Weihe, L. Cronin, G. Rajaraman, D. Collison, E. J. L. McInnes and R. E. P. Winpenny, *PNAS*, 2012, **109**, 19113–19118.

6 S. J. Shah, C. M. Ramsey, K. J. Heroux, J. R. O'Brien, A. G. DiPasquale, A. L. Rheingold, E. del Barco and D. N. Hendrickson, *Inorg. Chem*., 2008, **47**, 6245–6253.

7 G. A. Timco, T. B. Faust, F. Tuna and R. E. P. Winpenny, *Chem. Soc. Rev*., 2011, **40**, 3067-3075.

8 H. W. L. Fraser, G. S. Nichol, D. Uhrín, U. G. Nielsen, M. Evangelisti, J. Schnack and E.K. Brechin, *Dalton Trans*., 2018, **47**, 15530-15537.

9 A. J. Tasiopoulos, A. Vinslava, W. Wernsdorfer, K. A. Abboud and G. Christou, *Angew. Chem. Int. Ed*., 2004, **43**, 2117-2121.

10 C. Papatriantafyllopoulou, E. E Moushi, G. Christou and A. J Tasiopoulos, *Chem. Soc. Rev*., 2016, **45**, 1597-1628.

11 M. Manoli, R. Inglis, S. Piligkos, L. Yanhua, W. Wernsdorfer, E. K. Brechin and A. J. Tasiopoulos, *Chem. Commun*., 2016, **52**, 12829-12832.

12 S. Zartilas, C. Papatriantafyllopoulou, T. C. Stamatatos, V. Nastopoulos, E. Cremades, E. Ruiz, G. Christou, C. Lampropoulos and A. J. Tasiopoulos, *Inorg. Chem*., 2013, **52**, 12070–12079.

13 M. Manoli, R. Inglis, M. J. Manos, V. Nastopoulos, W. Wernsdorfer, E. K. Brechin and A. J. Tasiopoulos, *Angew. Chem. Int. Ed*., 2011, **50**, 4441-4444.

14 A. J. Tasiopoulos and S. P. Perlepes, *Dalton Trans*., 2008, 5537-5555.

15 M. V. Baker, D. H. Brown, B. W. Skelton and A. H. White, *J. Chem. Soc., Dalton Trans*., 1999, 1483-1490.

16 M. Riaz, R. K. Gupta, H.-F. Su, Z. Jagličić, M. Kurmoo, C.-H. Tung, D. Sun and L.-S. Zheng, *Inorg. Chem*., 2019, **58**, 14331-14337.

17 T. G. Tziotzi, M. Coletta, M. Gray, C. L. Campbell, S. J. Dalgarno, G. Lorusso, M. Evangelisti, E. K. Brechin and C. J. Milios, *ChemRxiv*, https://doi.org/10.26434/chemrxiv.13416881.v1.

18 a) M. K. Singh and G. Rajaraman, Inorg. Chem., 2019, 58, 3175-3188; b) C. McDonald, S. Sanz, E. K. Brechin, M. K. Singh, G. Rajaraman, D. Gaynor and L. F. Jones, RSC Adv., 2014, 4, 38182; c) A. E. Dearle, D. J. Cutler, H. W. L. Fraser, S. Sanz, E. Lee, S. Dey, I. F. Diaz-Ortega, G. S. Nichol, H. Nojiri, M. Evangelisti, G. Rajaraman, J. Schnack, L. Cronin and E. K. Brechin, *Angew. Chem. Int. Ed*., 2019, **58**, 16903-16906.

19 N. Berg, T. Rajeshkumar, S. M. Taylor, E. K. Brechin, G. Rajaraman and L. F. Jones, *Chem. - Eur. J*., 2012, **18**, 5906.

20 a) R. Maurice, C. de Graaf and N. Guihéry, J. Chem. Phys., 2010, 133, 084307; b) K. R. Vignesh, S. K. Langley, C. J. Gartshore, B. Moubaraki, K. S. Murray and G. Rajaraman, *Inorg. Chem*., 2017, **56**, 1932-1949; c) K. R. Vignesh, S. K. Langley, C. J. Gartshore, I. Borilović, C. M. Forsyth, G. Rajaraman and K. S. Murray, Dalton Trans., 2018, 47, 11820-11833; d) K. R. Vignesh, S. K. Langley, K. S. Murray and G. Rajaraman, *Chem. – Eur. J*., 2015, **21**, 2881-2892.

21 M. Coletta, S. Sanz, D. J. Cutler, S. J. Teat, K. J. Gagnon, M. K. Singh, E. K. Brechin and S. J. Dalgarno, *Dalton Trans*., 2020, **49**, 14790-14797.

Supplementary Information

Synthesis of $[Mn^{III}_{12}Mn^{II}_{6}(O)_6(OH)_2(OMe)_6(L)_4(LH)_2Br_{12}]$ (1)

$MnBr_2{\cdot}4H_2O$ (143.4 mg, 0.5 mmol) was added to 10 mL of a 0.05 M solution of LH_3 in MeOH. Upon the addition, the solution turns brown. The solution was stirred for 30 minutes after which it was filtered and allowed to stand. Dark black crystals suitable for *X*-ray analysis grew after two days. Elemental Analysis (%) calculated for **1**, $C_{70}H_{170}Mn_{18}N_{18}O_{42}Br_{12}$ (*M* = 3884.07): C, 21.65%; H, 4.41%; N, 3.26%. Found: C, 21.37%; H, 4.28%; N, 3.05%. Yield: 39 mg (2%).

Crystallographic data

Crystal data for **1** (CCDC 2054790): $C_{70}H_{170}Mn_{18}N_{18}O_{42}Br_{12}$, *M* = 3884.07, 0.05 × 0.05 × 0.02 mm^3, monoclinic, space group *I*2/*a* (No. 15), a = 18.408(6) Å, b = 23.209(7) Å, c = 30.524(12) Å, β = 90.126(5)°, $\alpha = \gamma = 90°$, *V* = 13041(7) $Å^3$, *T* = 100.0 K, *Z* = 4. Diamond Light Source I-19 EH1 diffractometer,[1] synchrotron radiation, λ = 0.68890 Å, T = 100.00 K, 2ϑmax = 40.249°, 46537 reflections measured, 6837 unique (R_{int} = 0.0984) which were used in all calculations. Final GooF = 1.071, wR_2 was 0.3459 (all data) and R_1 was 0.1163 (I≥2 σ(I)).

Magnetometry

Dc magnetic susceptibility and magnetisation measurements were performed on a freshly prepare microcrystalline, powdered sample of **1** on a Quantum Design SQUID MPMS-XL magnetometer equipped with a 7T magnet. Unit cell parameters were checked prior to sample preparation.

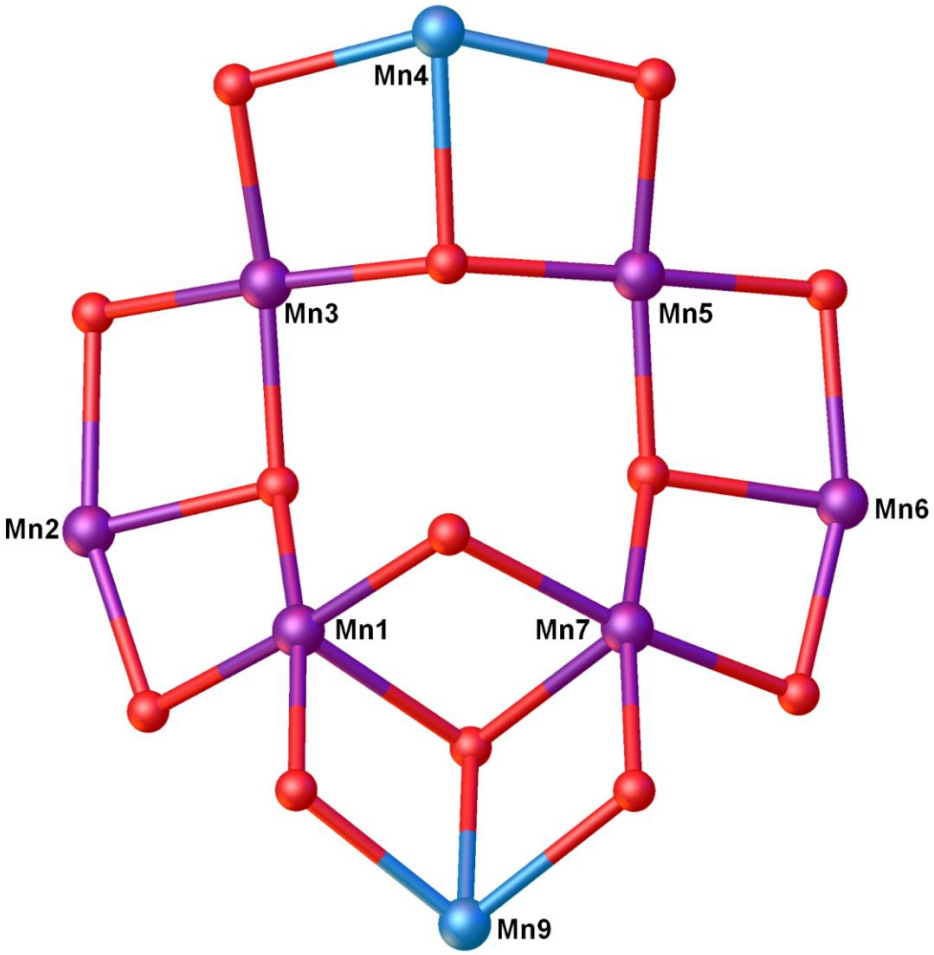

Figure S1. Metallic skeleton of the labelled ASU of **1**. Colour code: Mn^{III} = purple, Mn^{II} = light blue, O = red.

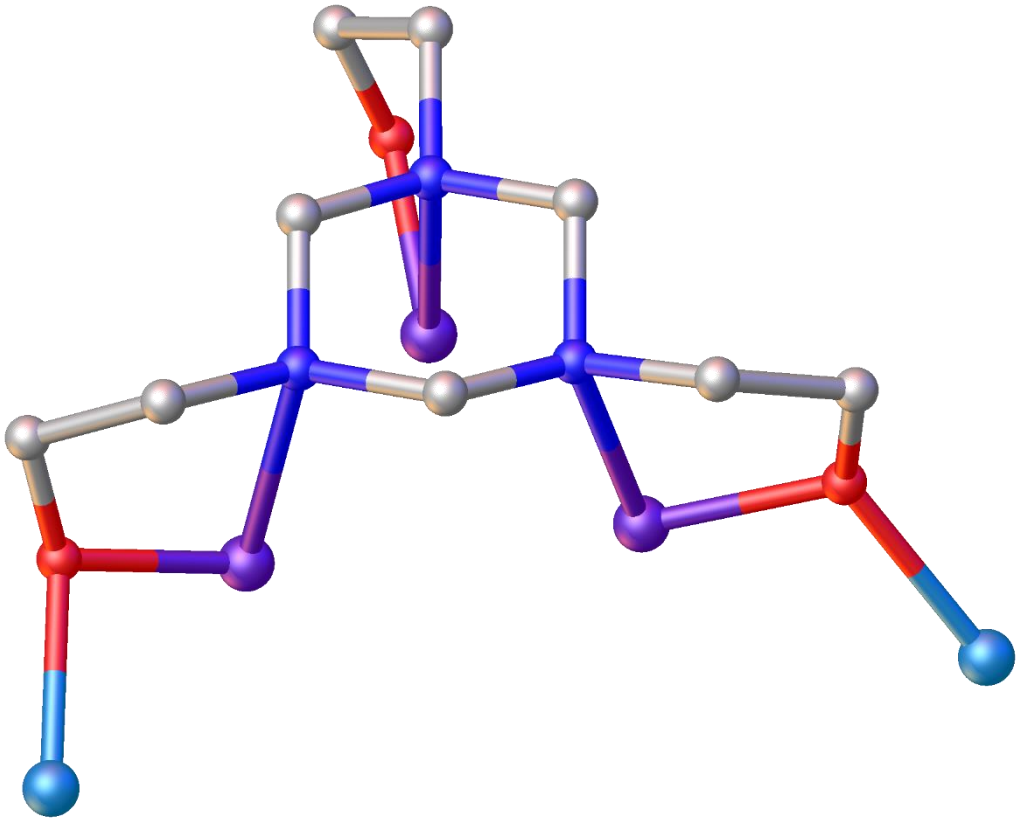

Figure S2. View of the coordination mode of the L^{3-} ligand. Colour code: Mn^{III} = purple, Mn^{II} = blue, C = grey, O = red, N = dark blue. H atoms omitted for clarity.

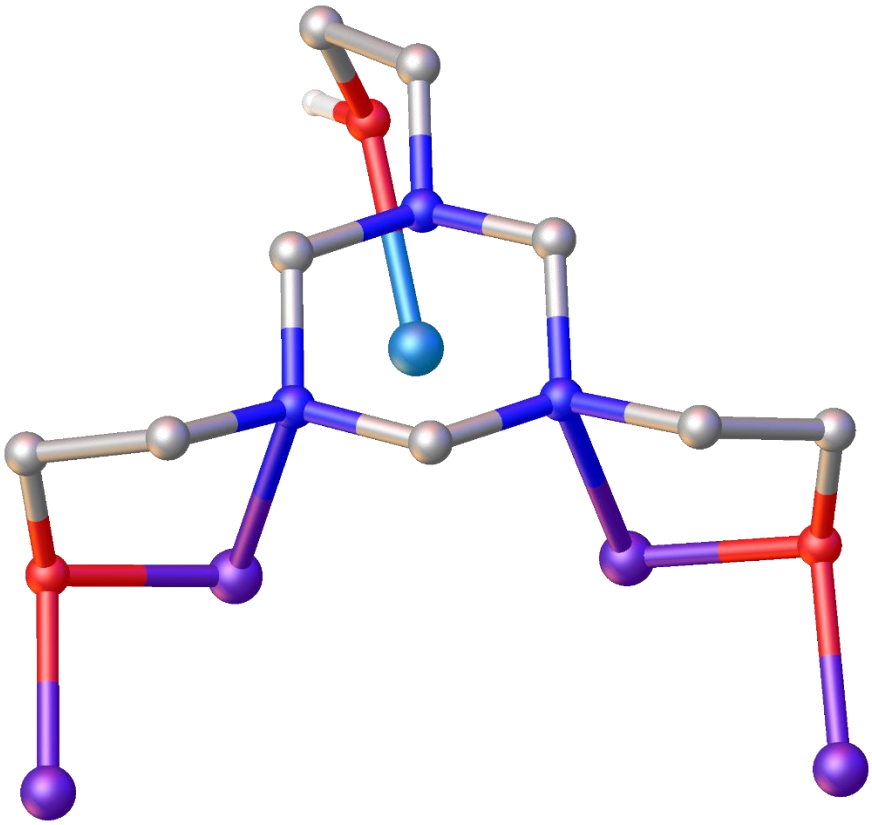

Figure S3. View of the coordination mode of the LH^{2-} ligand. Colour code: Mn^{III} = purple, Mn^{II} = blue, C = grey, O = red, N = dark blue. H atoms omitted for clarity.

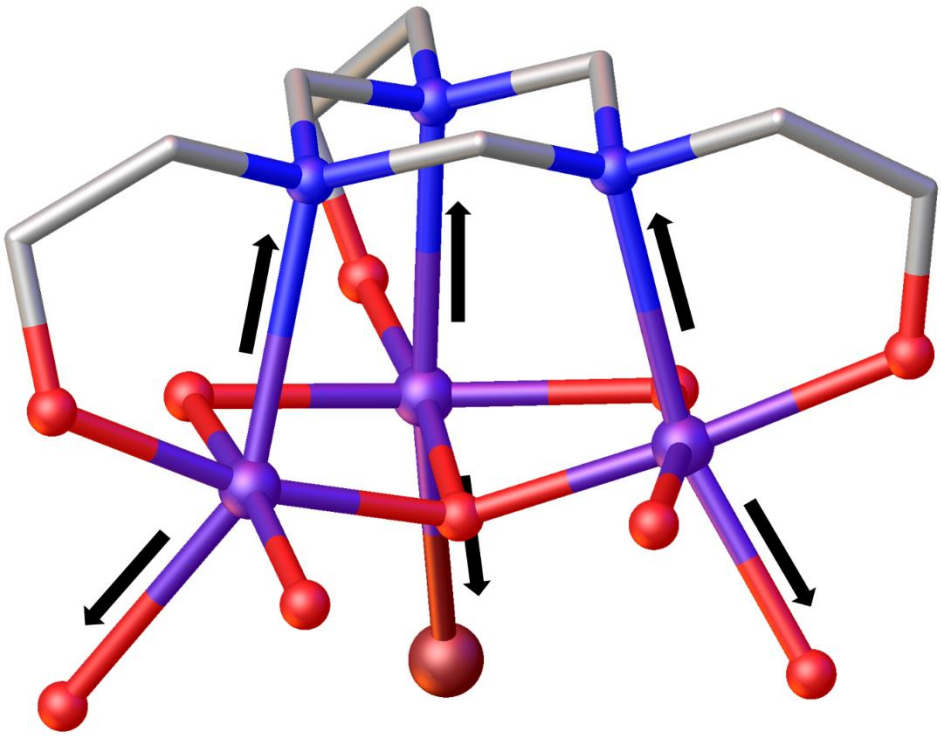

Figure S4. View of the L^{3-} ligand sitting above a [Mn^{III}_3] triangle. The arrows highlight the Jahn-Teller axes. Colour code: Mn^{III} = purple, C = grey, O = red, N = dark blue, Br = brown. H atoms omitted for clarity.

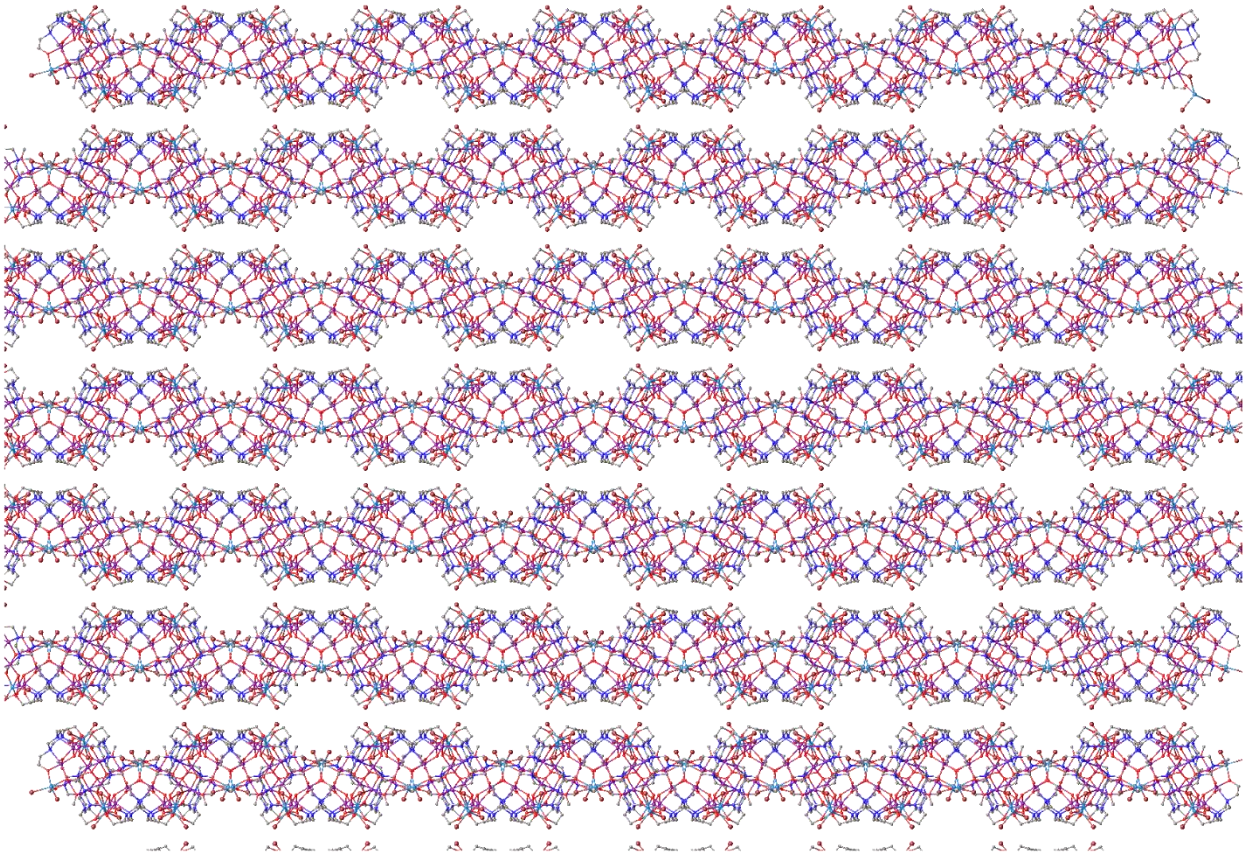

Figure S5. View of the extended structure of **1** in the *bc* plane showing the column-like arrangement of the molecules.

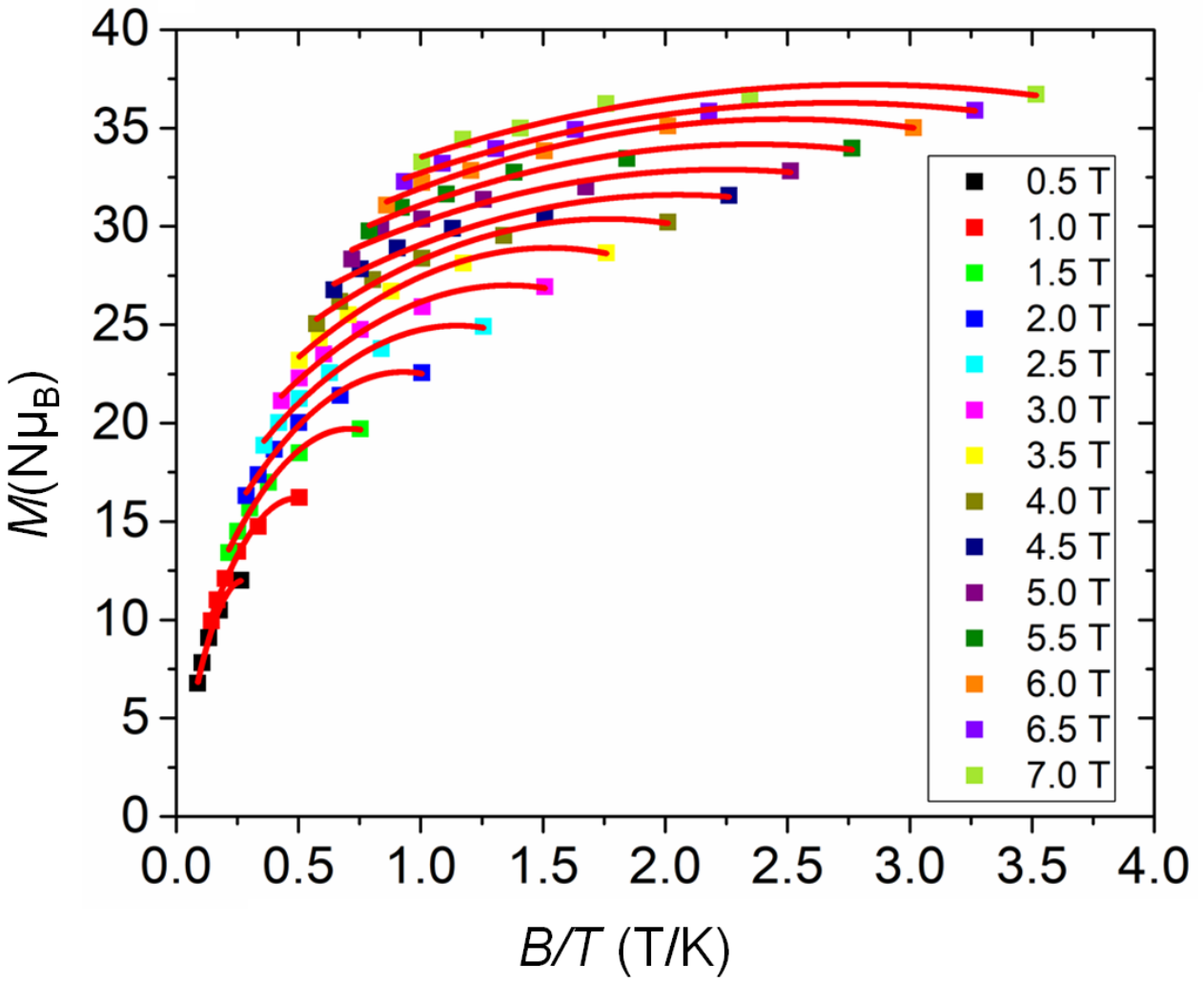

Figure S6. Plot of the reduced magnetisation (*M*) vs (*B*/*T*) for compound **1** in *B* = 0.5-7 T. The red lines are a guide to the eye, not a fit of the data.

COMPUTATIONAL DETAILS

We have used density functional theory (DFT) in the Gaussian 16 suite to estimate the magnetic exchange coupling constants (J_1-J_6) for **1**.[2] We have performed calculations on model complex **1a** based on the ASU of **1** (Mn_9, Figure S7). For the calculation of each interaction we have used the diamagnetic substitution method by keeping only the two paramagnetic ions of interest and replacing all others with diamagnetic ions (Ga^{III} and Zn^{II} for Mn^{III} and Mn^{II}, respectively). By doing so, we keep the ligand field around the paramagnetic metals ions identical to **1**. This method is known to yield reliable magnetic exchange coupling values for molecular systems with relatively small magnetic interactions.[3] Noodleman's broken symmetry approach[4] has been used to estimate the magnetic exchange coupling constants. We have used the B3LYP functional[5] together with Ahlrichs TZV basis set[6] for Mn, Ga, Zn; the SDD basis set[7] (which combines DZ with the Stuttgart-Dresden ECP basis set) for Br and the 6-31G** basis set[8] for O, N, C and H. This methodology has been known to yield excellent estimates of *J* values for 3d metal clusters.[3b,9]

Table S1. DFT computed magnetic exchange interactions together with pertinent structural parameters for **1**.

Exchange		Bridging groups	Mn···Mn Dist. [Å]	Avg. Mn-O Dist. [Å]	Avg. Mn-O-Mn angle [º]	*J* cm^{-1}
	Mn_{12}	μ_3-O, μ-OR	2.94	1.94	99	-10
	Mn_{23}	μ_3-O, μ-OR	3.00	1.98	99	
J_1	Mn_{56}	μ_3-O, μ-OR	2. 99	1.96	100	
	Mn_{67}	μ_3-O, μ-OR	2.96	1.97	98	
	Mn_{13}	μ_3-O	3.46	1.89	133	-9
	Mn_{35}	μ_3-O	3.52	1.90	136	
J_2	Mn_{57}	μ_3-O	3.48	1.90	132	
J_3	Mn_{17}	μ-OH, μ_3-OR	3.10	2.03	98	+8
J_4	Mn_{34}	μ_3-O, μ-OR	3.06	2.03	98	+1
	Mn_{45}	μ_3-O, μ-OR	3.10	2.04	99	
J_5	Mn_{19}	μ-OR, μ_3-OR	3.25	2.11	102	+2
	Mn_{79}	μ-OR, μ_3-OR	3.24	2.10	101	
J_6	Mn_{68}	μ-Br, μ-OR	3.58	2.42	102	+2

Table S2. DFT computed overlap integral (OI) values for J_1-J_6. Here α and β signify spin-up and spin-down orbitals, respectively. $\sum|S_{a(3d)b(3d)}|$ represents the total OIs and $\sum|S_{a(3d)b(3d)}|/n$ represents the average total OIs between Mn^{III}-Mn^{III}/Mn^{II}-Mn^{III} SOMOs. n = number of possible OIs between the SOMOs (for $3d^4$-$3d^4$ systems, n = 16 and for $3d^5$-$3d^4$ systems, n = 20). Red and yellow highlighted numbers represent strong and intermediate interactions, respectively.

						$\sum\|S_{a(3d)b(3d)}\|$	$\sum\|S_{a(3d)b(3d)}\|/n$
J_1	β(→)/α(↓)	d_{xz}	d_{xy}	d_{yz}	d_z^2		
	d_{xy}	0.025	0.023	0.026	0.069	0.708	0.044
	d_{xz}	0.066	0.027	0.001	0.001		
	d_{yz}	0.049	0.014	0.057	0.001		
	d_z^2	0.137	0.072	0.100	0.040		
J_2	β(→)/α(↓)	d_{xz}	d_{yz}	d_{xy}	d_z^2		
	d_{xy}	0.054	0.012	0.044	0.042	0.572	0.036
	d_{xz}	0.005	0.057	0.001	0.058		
	d_{yz}	0.005	0.006	0.022	0.135		
	d_z^2	0.018	0.032	0.003	0.078		
J_3	β(→)/α(↓)	d_{xz}	d_{yz}	d_{xy}	d_z^2		
	d_{xy}	0.003	0.004	0.052	0.070	0.338	0.021
	d_{xz}	0.002	0.005	0.015	0.016		
	d_{yz}	0.016	0.012	0.019	0.012		
	d_z^2	0.068	0.009	0.024	0.011		
J_4	β(→)/α(↓)	d_{xy}	d_{xz}	d_{yz}	d_z^2		
	d_{xz}	0.027	0.081	0.052	0.036	0.624	0.031
	d_{yz}	0.030	0.030	0.020	0.018		
	d_{xy}	0.036	0.008	0.023	0.079		
	d_z^2	0.013	0.048	0.058	0.045		
	$d_{x^2-y^2}$	0.004	0.006	0.009	0.001		
J_5	β(→)/α(↓)	d_{xy}	d_{xz}	d_{yz}	d_z^2		
	d_{xz}	0.012	0.017	0.011	0.068	0.467	0.023
	d_{xy}	0.011	0.088	0.011	0.010		
	d_{yz}	0.038	0.032	0.026	0.004		
	d_z^2	0.006	0.000	0.031	0.025		
	$d_{x^2-y^2}$	0.045	0.038	0.020	0.057		
J_6	β(→)/α(↓)	d_{xz}	d_{xy}	d_{yz}	d_z^2		
	d_{xy}	0.025	0.001	0.007	0.004	0.490	0.025
	d_{xz}	0.001	0.027	0.009	0.009		
	$d_{x^2-y^2}$	0.009	0.039	0.017	0.013		
	d_{yz}	0.082	0.035	0.012	0.016		
	d_z^2	0.015	0.026	0.038	0.105		

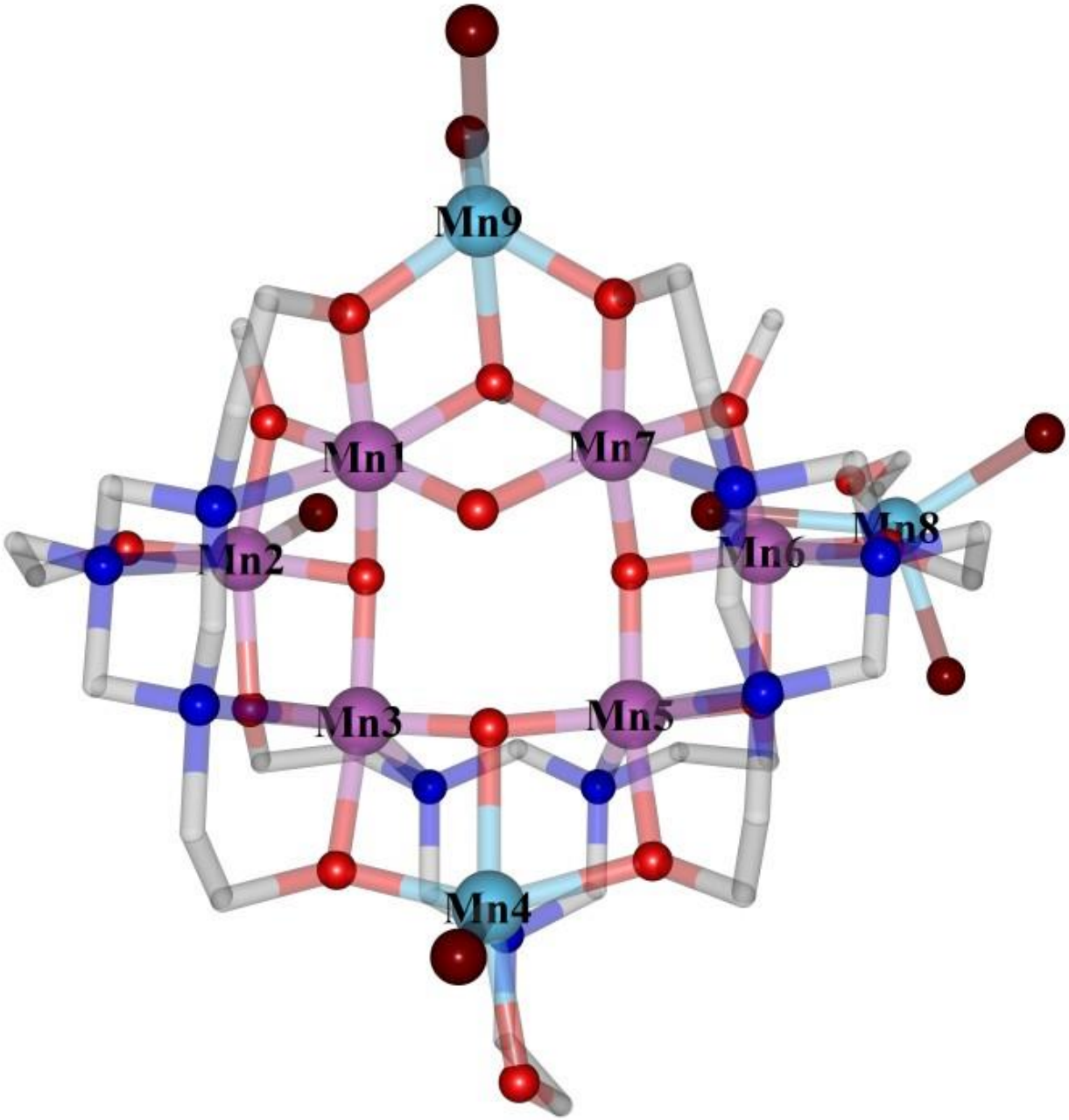

Figure S7. The structure of model complex **1a** on which DFT calculations were performed to estimate the magnetic exchange coupling constants. H-atoms are removed for clarity (except the μ-OH bridging group). Colour code is the same as for Figure 2.

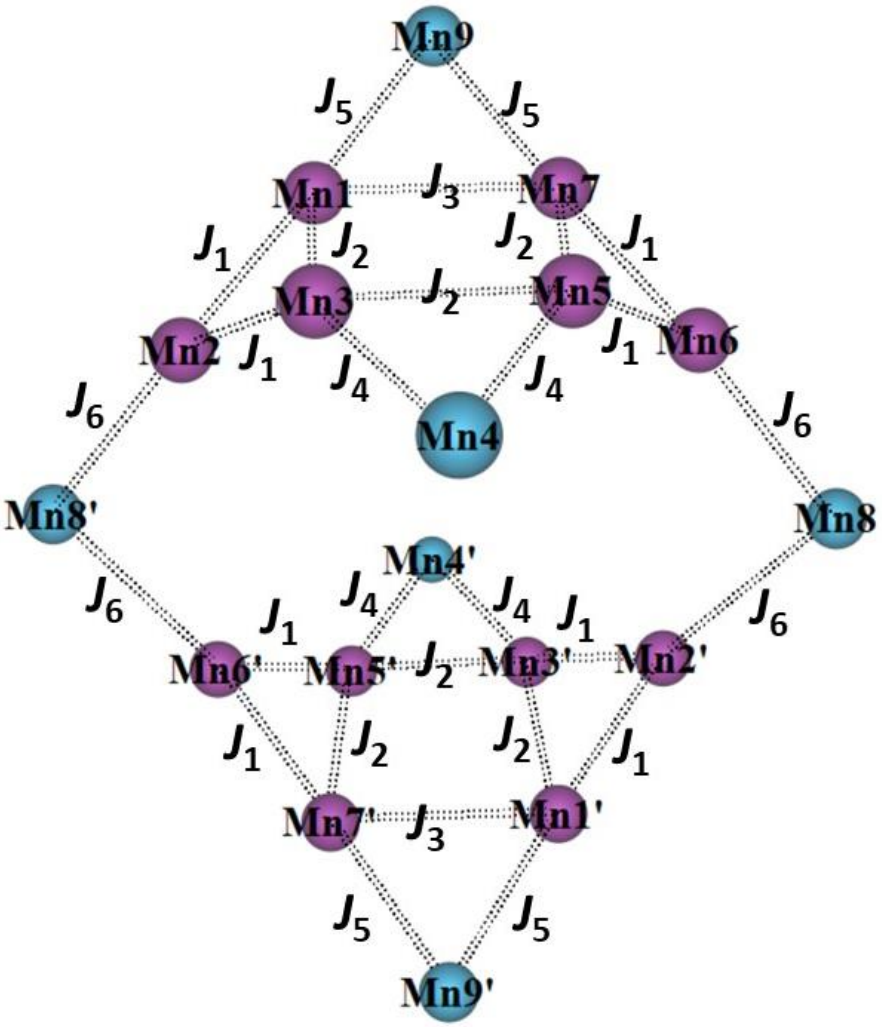

$\hat{H}$ = -2J_1($\hat{S}_{Mn1}\hat{S}_{Mn2}$ + $\hat{S}_{Mn2}\hat{S}_{Mn3}$ + $\hat{S}_{Mn5}\hat{S}_{Mn6}$ + $\hat{S}_{Mn6}\hat{S}_{Mn7}$ + $\hat{S}_{Mn1'}\hat{S}_{Mn2'}$ + $\hat{S}_{Mn2'}\hat{S}_{Mn3'}$ + $\hat{S}_{Mn5'}\hat{S}_{Mn6'}$ + $\hat{S}_{Mn6'}\hat{S}_{Mn7'}$) - 2$J_2$($\hat{S}_{Mn1}\hat{S}_{Mn3}$ + $\hat{S}_{Mn3}\hat{S}_{Mn5}$ + $\hat{S}_{Mn5}\hat{S}_{Mn7}$ + $\hat{S}_{Mn1'}\hat{S}_{Mn3'}$ + $\hat{S}_{Mn3'}\hat{S}_{Mn5'}$ + $\hat{S}_{Mn5'}\hat{S}_{Mn7'}$) -2$J_3$($\hat{S}_{Mn1}\hat{S}_{Mn7}$ + $\hat{S}_{Mn1'}\hat{S}_{Mn7'}$) - 2$J_4$($\hat{S}_{Mn3}\hat{S}_{Mn4}$ + $\hat{S}_{Mn4}\hat{S}_{Mn5}$ + $\hat{S}_{Mn3'}\hat{S}_{Mn4'}$ + $\hat{S}_{Mn4'}\hat{S}_{Mn5'}$) -2$J_5$($\hat{S}_{Mn1}\hat{S}_{Mn9}$ + $\hat{S}_{Mn7}\hat{S}_{Mn9}$ + $\hat{S}_{Mn1'}\hat{S}_{Mn9'}$ + $\hat{S}_{Mn7'}\hat{S}_{Mn9'}$) - 2$J_6$($\hat{S}_{Mn2}\hat{S}_{Mn8}$ + $\hat{S}_{Mn6}\hat{S}_{Mn8}$ + $\hat{S}_{Mn2'}\hat{S}_{Mn8'}$ + $\hat{S}_{Mn6'}\hat{S}_{Mn8'}$)

Figure S8. Schematic representation of the six different exchange interactions present in **1**, together with the exchange part of the corresponding spin-Hamiltonian.

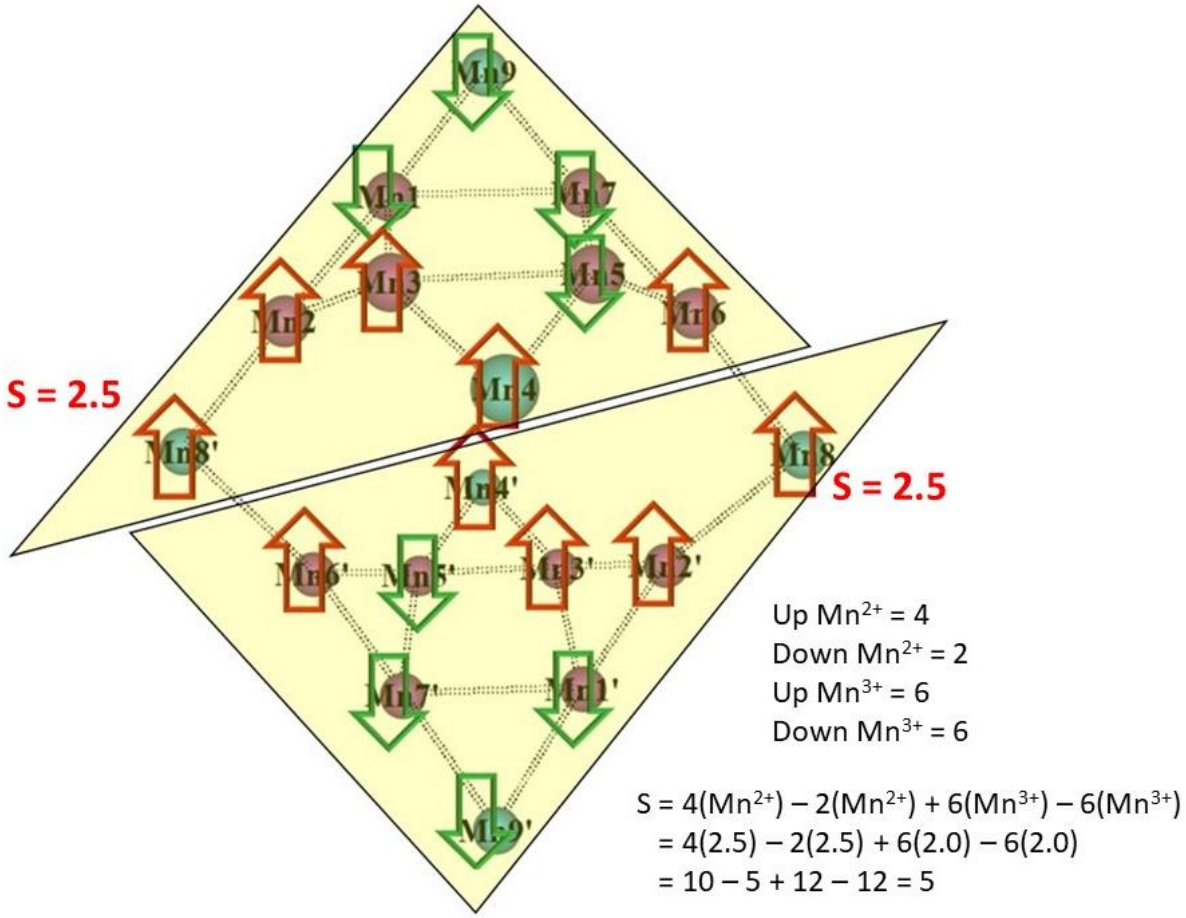

Figure S9. Schematic presentation of spin orientation for **1** based on the DFT calculated *J* values. Red and green arrows represent spin-up and spin-down, respectively. Calculation suggest *S* = 5 as the ground spin state with strong spin frustration.

(a)

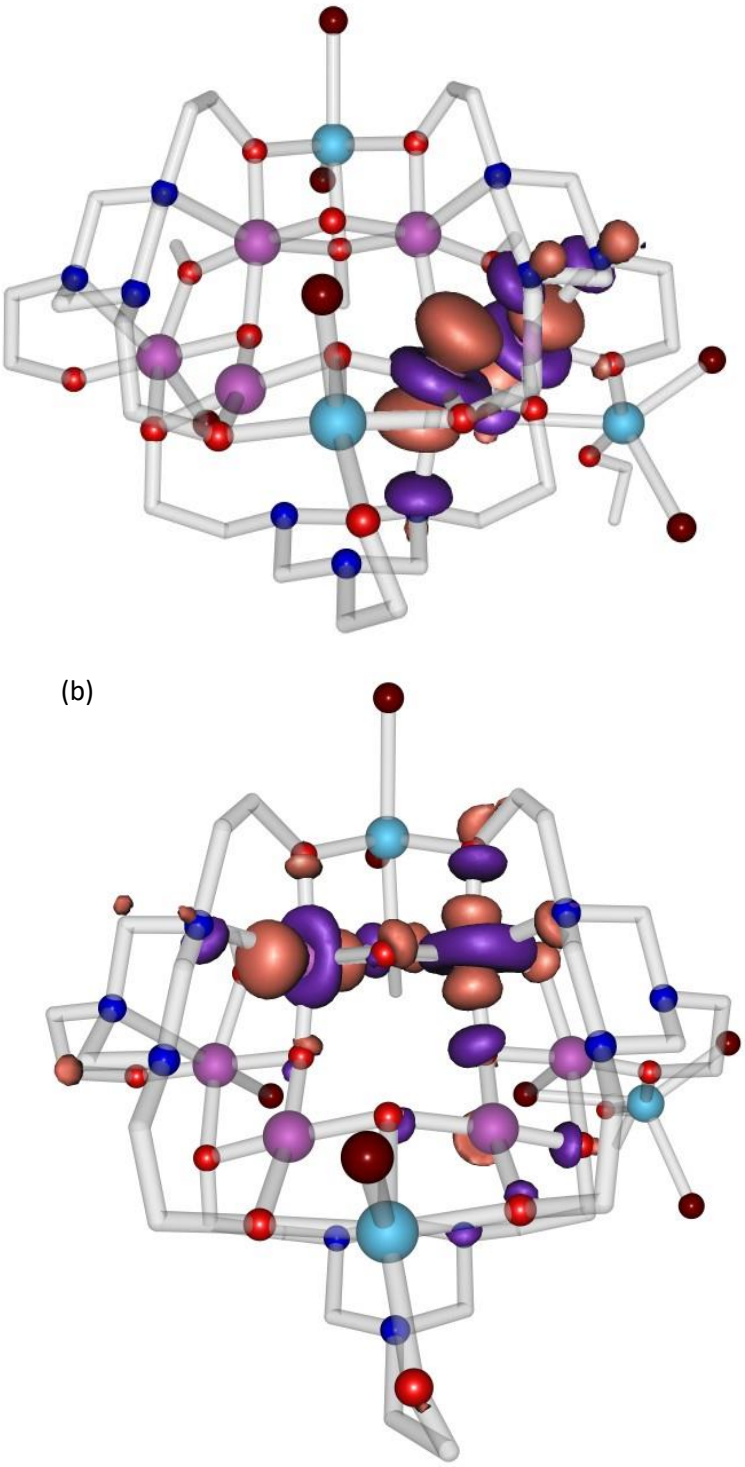

Figure S10. Schematic presentation of Jahn-Teller axis for (a) {Mn5-Mn6, J_1} and (b) {Mn1-Mn7, J_3} centres within the ASU. For J_1 the Jahn-Teller axis of both Mn^{III} ions are found to be collinear and are perpendicular to the bridging plane of the dimer (Type I). For J_3 interaction, the Jahn-Teller axes of Mn^{III} ions are perpendicular to each other with one lying parallel to the bridging plane and the other perpendicular to the bridging plane (Type III).[10]

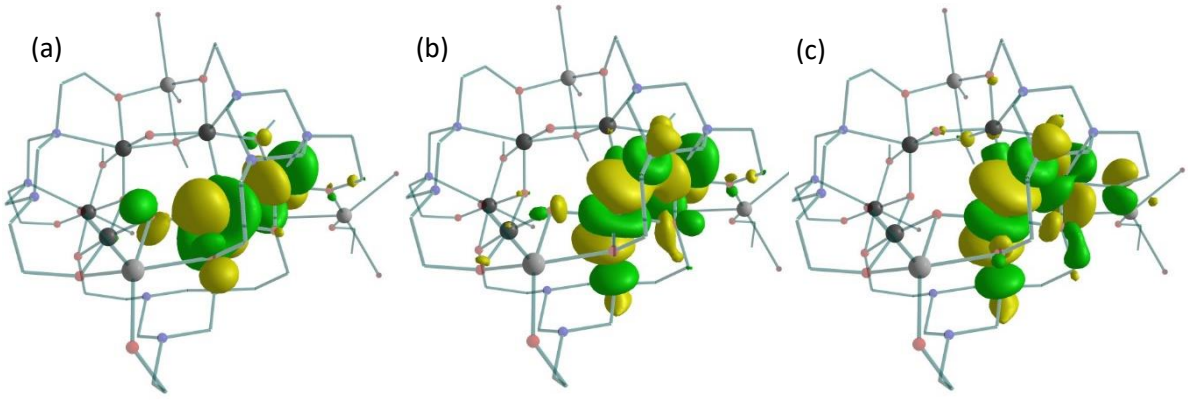

$Mn5(d_{xz})|p|Mn6(d_{xz}) = 0.066$ $Mn5(d_{z^2})|p|Mn6(d_{xz}) = 0.137$ $Mn5(d_{z^2})|p|Mn6(d_{xy}) = 0.072$

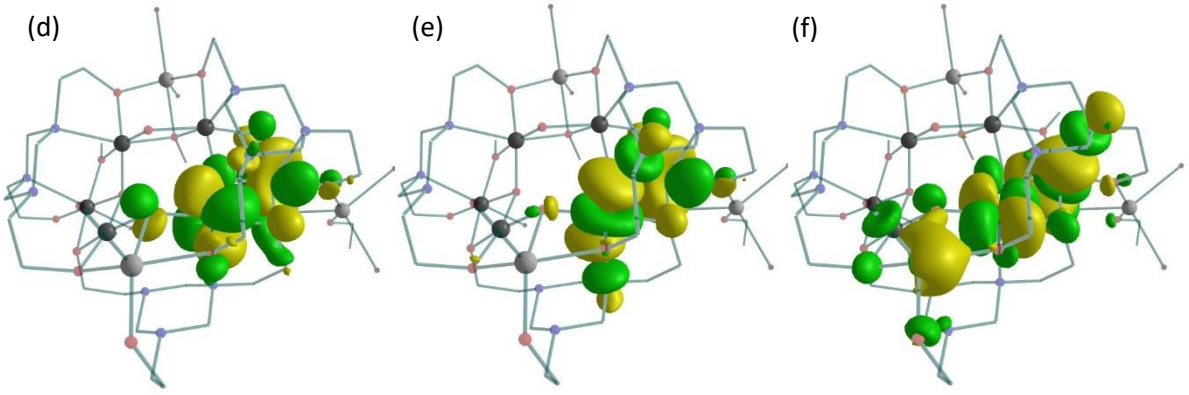

$Mn5(d_{yz})|p|Mn6(d_{yz}) = 0.057$ $Mn5(d_{z^2})|p|Mn6(d_{yz}) = 0.100$ $Mn5(d_{xy})|p|Mn6(d_{z^2}) = 0.069$

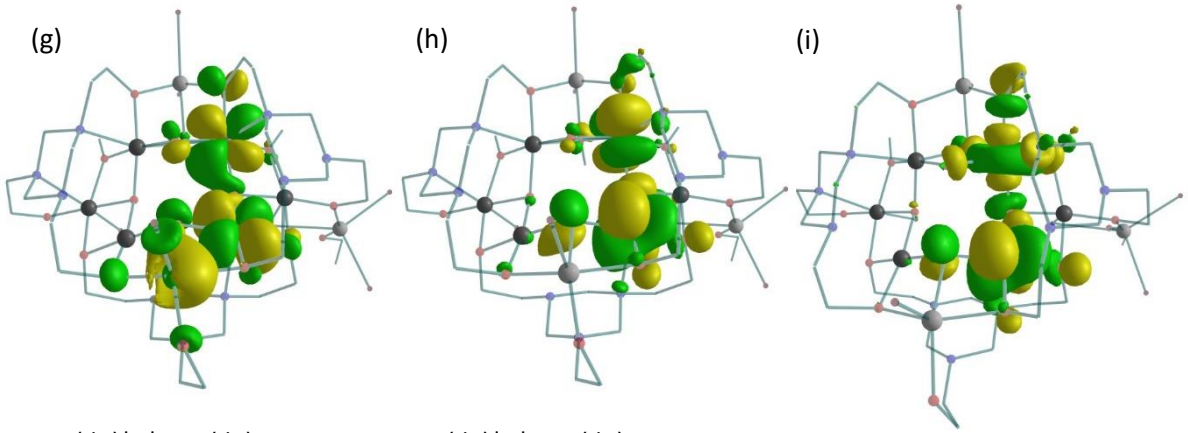

$Mn5(d_{xy})|p|Mn7(d_{xz}) = 0.054$ $Mn5(d_{xz})|p|Mn7(d_{yz}) = 0.057$ $Mn5(d_{xz})|p|Mn7(d_{z^2}) = 0.058$

(j)

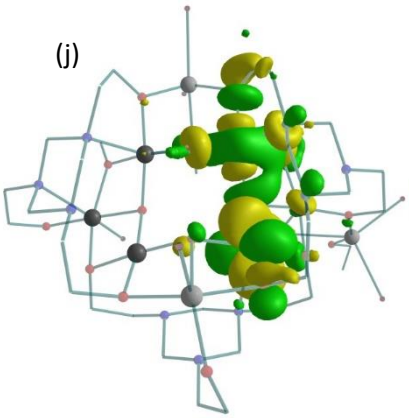

$Mn5(d_{yz})|p|Mn7(d_{z^2}) = 0.135$

(k)

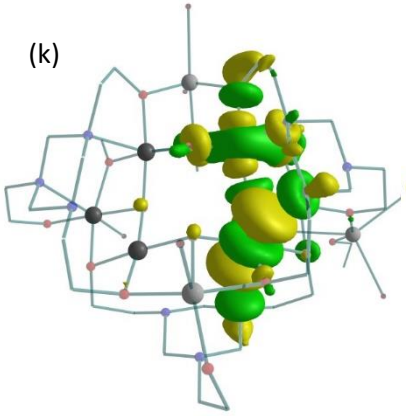

$Mn5(d_{z^2})|p|Mn7(d_{z^2}) = 0.078$

(l)

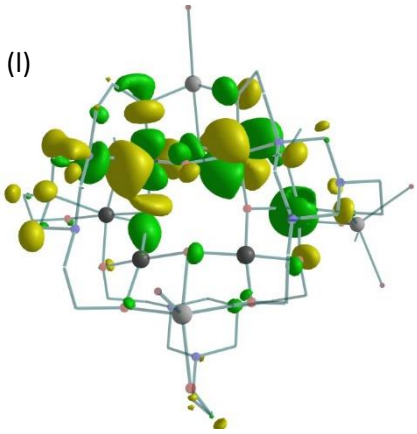

$Mn1(d_{z^2})|p|Mn7(d_{xz}) = 0.068$

(m)

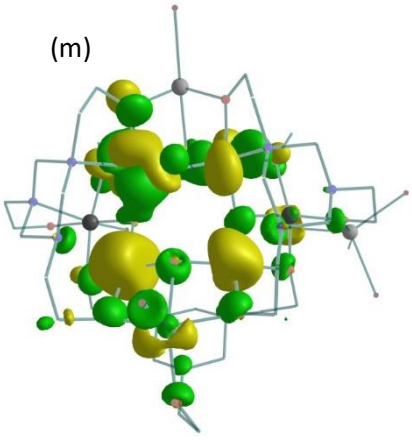

$Mn1(d_{xy})|p|Mn7(d_{xy}) = 0.052$

(n)

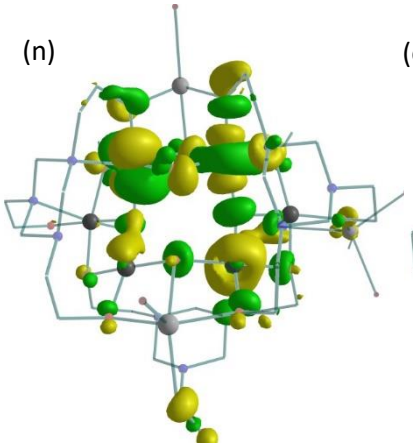

$Mn1(d_{xy})|p|Mn7(d_{z^2}) = 0.070$

(o)

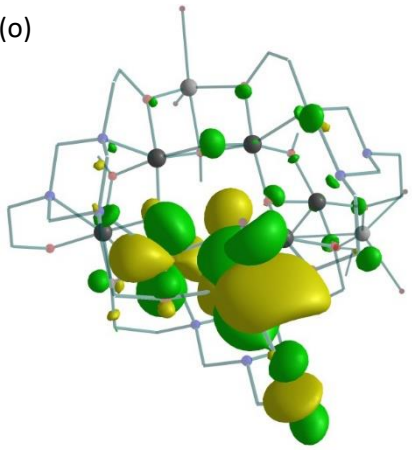

$Mn4(d_{xz})|p|Mn3(d_{xz}) = 0.081$

(p)

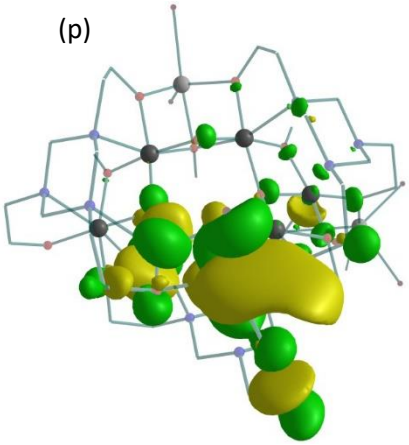

$Mn4(d_{xz})|p|Mn3(d_{yz}) = 0.052$

(q)

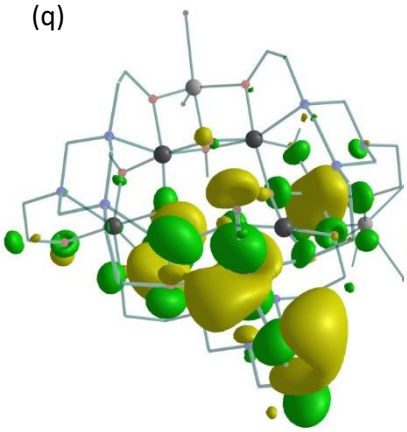

$Mn4(d_{z^2})|p|Mn3(d_{yz}) = 0.058$

(r)

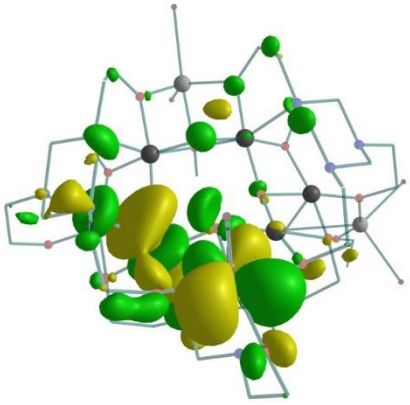

$Mn4(d_{xy})|p|Mn3(d_{z^2}) = 0.079$

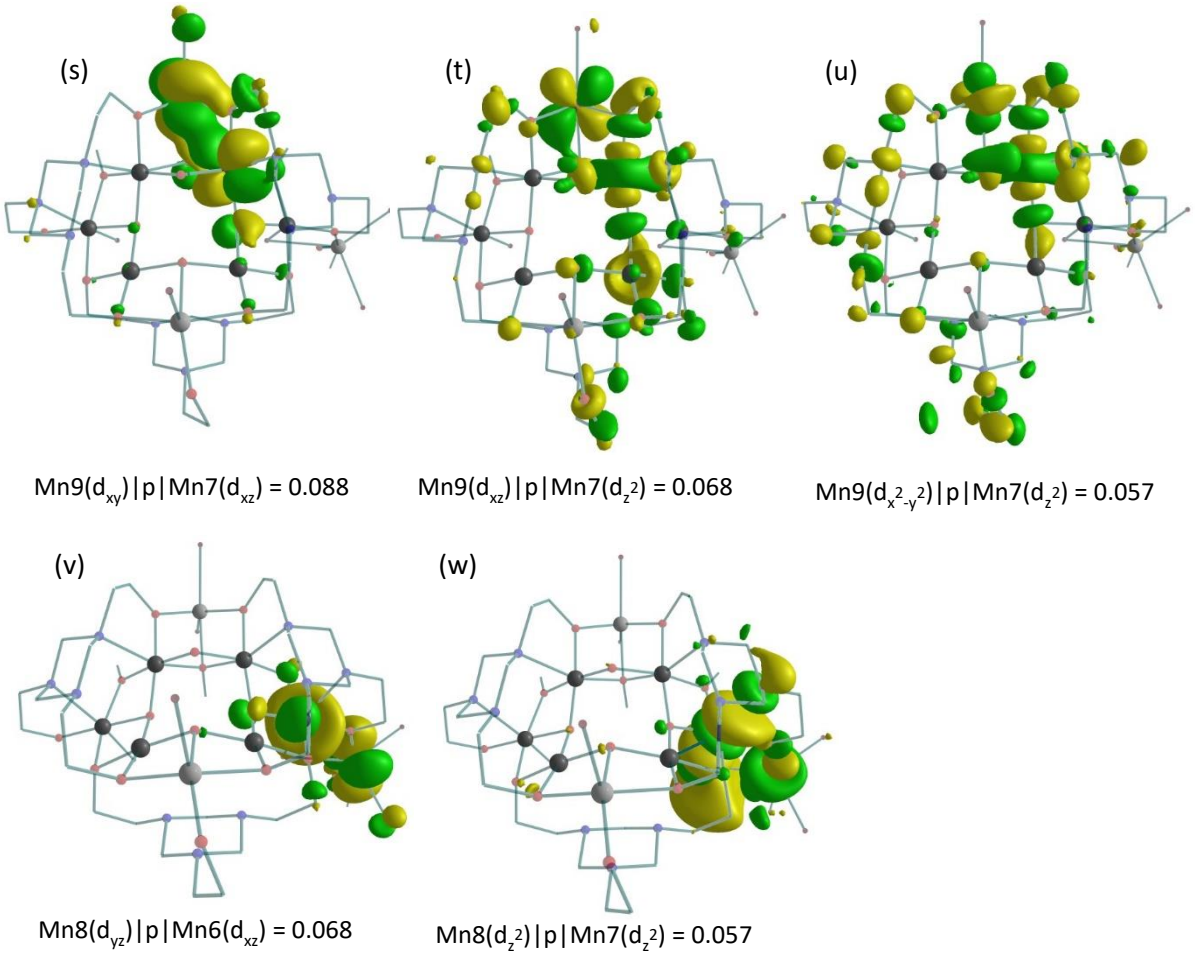

Figure S11. DFT calculated strong and intermediate overlap integrals corresponding to (a-f) J_1; (g-k) J_2; (l-n) J_3; (o-r) J_4; (s-u) J_5 and (v-w) J_6.

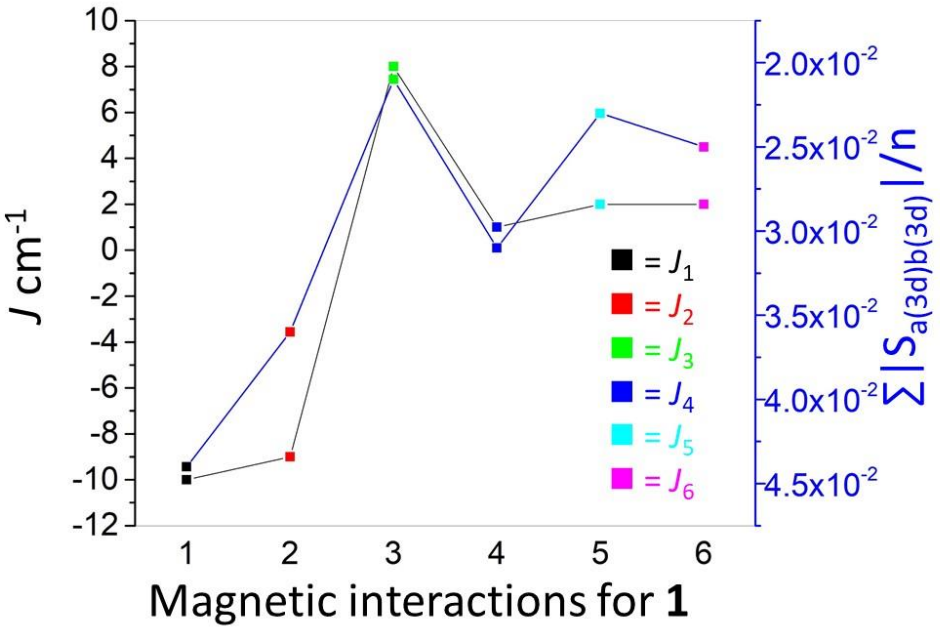

Figure S12. Plot of *J* versus average total overlap integral ($\sum|S_{a(3d)b(3d)}|/n$) with respect to the calculated magnetic exchange interactions for **1**. The magnitude and the sign of the magnetic exchange interaction can be correlated to the calculated average total overlap integral. The smaller the average total overlap integral, the larger the ferromagnetic interaction and vice versa.[3a]

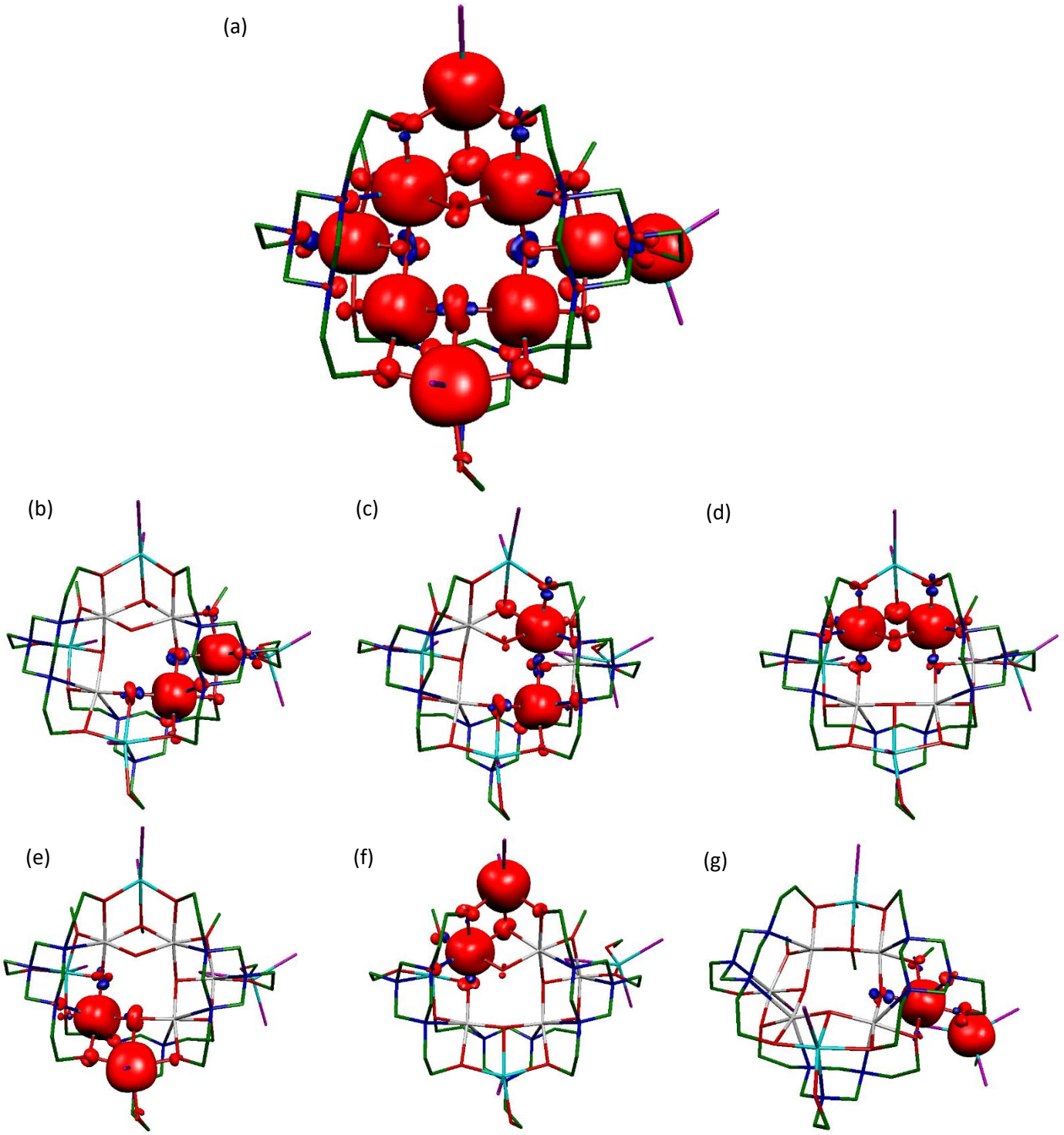

Figure S13. DFT calculated spin density plots for (a) model **1a** and (b-g) diamagnetic substituted models for J_1-J_6, respectively. The isodensity surfaces shown reflect a value of 0.01 e -/bohr^3. The red and blue surfaces denote positive and negative spin density, respectively.

References

1. N. T. Johnson, P. G. Waddell, W. Clegg and M. R. Probert, *Crystals*, 2017, **7**, 360.
2. M. J. Frisch, G. W. Trucks, H. B. Schlegel, G. E. Scuseria, M. A. Robb, J. R. Cheeseman, G. Scalmani, V. Barone, G. A. Petersson, H. Nakatsuji, X. Li, M. Caricato, A. V. Marenich, J. Bloino, B. G. Janesko, R. Gomperts, B. Mennucci, H. P. Hratchian, J. V. Ortiz, A. F. Izmaylov, J. L. Sonnenberg, Williams, F. Ding, F. Lipparini, F. Egidi, J. Goings, B. Peng, A. Petrone, T. Henderson, D. Ranasinghe, V. G. Zakrzewski, J. Gao, N. Rega, G. Zheng, W. Liang, M. Hada, M. Ehara, K. Toyota, R. Fukuda, J. Hasegawa, M. Ishida, T. Nakajima, Y. Honda, O. Kitao, H. Nakai, T. Vreven, K. Throssell, J. A. Montgomery Jr., J. E. Peralta, F. Ogliaro, M. J. Bearpark, J. J. Heyd, E. N. Brothers, K. N. Kudin, V. N. Staroverov, T. A. Keith, R. Kobayashi, J. Normand, K. Raghavachari, A. P. Rendell, J. C. Burant, S. S. Iyengar, J. Tomasi, M. Cossi, J. M. Millam, M. Klene, C. Adamo, R. Cammi, J. W. Ochterski, R. L. Martin, K. Morokuma, O. Farkas, J. B. Foresman and D. J. Fox, Gaussian, Inc., Wallingford CT, 2016.
3. a) M. Coletta, S. Sanz, D. J. Cutler, S. J. Teat, K. J. Gagnon, M. K. Singh, E. K. Brechin and S. J. Dalgarno, *Dalton Trans.*, 2020, **49**, 14790-14797; b) A. E. Dearle, D. J. Cutler, H. W. L. Fraser, S. Sanz, E. Lee, S. Dey, I. F. Diaz-Ortega, G. S. Nichol, H. Nojiri, M. Evangelisti, G. Rajaraman, J. Schnack, L. Cronin and E. K. Brechin, *Angew. Chem. Int. Ed.*, 2019, **58**, 16903-16906.
4. L. Noodleman, *J. Chem. Phys.*, 1981, **74**, 5737.
5. a) A. D. Becke, *Phys. Rev. A*, 1988, **38**, 3098-3101; b) A. D. Becke, *J. Chem. Phys.*, 1993, **98**, 5648; c) C. Lee, W. Yang and R. G. Parr, *Phys. Rev. B: Condens. Matter Mater. Phys.*, 1988, **37**, 785.
6. a) A. Schafer, H. Horn and R. Ahlrichs, *J. Chem. Phys.*, 1992, **97**, 2571-2577; b) A. Schäfer, C. Huber and R. Ahlrichs, *J. Chem. Phys.*, 1994, **100**, 5829; c) G. E. Scuseria and H. F. Schäfer, *J. Chem. Phys.*, 1989, **90**, 3700.
7. A. Bergner, M. Dolg, W. Küchle, H. Stoll and H. Preuß, *Mol. Phys.*, 1993, **80**, 1431-1441.
8. V. A. Rassolov, J. A. Pople, M. A. Ratner and T. L. Windus, *J. Chem. Phys.*, 1998, **109**, 1223-1229.
9. a) M. K. Singh, *Dalton Trans.*, 2020, **49**, 4539-4548; b) M. K. Singh and G. Rajaraman, *Inorg. Chem.*, 2019, **58**, 3175-3188; c) M. K. Singh and G. Rajaraman, *Chem. Eur. J.*, 2015, **21**, 980-983; d) J. Caballero-Jiménez, F. Habib, D. Ramírez-Rosales, R. Grande-Aztatzi, G. Merino, I. Korobkov, M. K. Singh, G. Rajaraman, Y. Reyes-Ortega and M. Murugesu, *Dalton Trans*, 2015, **44**, 8649; e) C. McDonald, S. Sanz, E. K. Brechin, M. K. Singh, G. Rajaraman, D. Gaynor and L. F. Jones, *RSC Adv.*, 2014, **4**, 38182.
10. N. Berg, T. Rajeshkumar, S. M. Taylor, E. K. Brechin, G. Rajaraman and L. F. Jones, *Chem. - Eur. J.*, 2012, **18**, 5906.